Am J Transl Res 2024;16(11):6615-6625
www.ajtr.org /ISSN:1943-8141/AJTR0159877

Original Article

Early precise screening of pulmonary nodules: risk factor analysis for malignant nodules

Qian Zhao[1], Teng Wang[2]

[1]Health Management Center, The First Affiliated Hospital of Air Force Military Medical University, Xi'an 710000, Shaanxi, China; [2]Health Management Center, Weinan Central Hospital, Weinan 714000, Shaanxi, China

Received August 17, 2024; Accepted October 16, 2024; Epub November 15, 2024; Published November 30, 2024

Abstract: Objectives: To analyze clinical data and CT imaging characteristics of patients with pulmonary nodules, clarifying the diagnostic value of CT features in distinguishing benign from malignant pulmonary nodules. To enhance diagnostic accuracy for pulmonary nodule characterization, assisting clinicians in diagnosis and providing optimal treatment recommendations. Methods: This retrospective study included 200 individuals who underwent dual-source CT lung cancer screening at the First Affiliated Hospital of Air Force Military Medical University from January 2023 to December 2023. Participants were categorized into benign and malignant groups based on pathological reports, with 102 cases in the benign group and 98 in the malignant group. Postoperative pathological outcomes were documented, and risk factors for lung cancer were analyzed, stratifying results by pathology and infiltration level. Results: Patients in the malignant group had significantly higher NICAp and CTAp values than those in the benign group (all $P < 0.05$). The diagnostic accuracy of chest CT for identifying benign vs. malignant nodules was 88.78%, with a sensitivity of 44.90% and a specificity of 57.84%. CT examination positivity was 42.16% in the benign group and 44.90% in the malignant group. Univariate and multivariate analyses identified NICAp (95% CI 1.045-1.367; $P = 0.007$), CTAp (95% CI 1.341-4.123; $P = 0.005$), solid nodule (95% CI 1.198-2.978; $P = 0.008$), and nodule density (95% CI 1.128-2.987; $P = 0.007$) as independent diagnostic factors for malignant nodules. Conclusion: NICAp, CTAp, solid nodule, and nodule density are independent diagnostic factors for malignant pulmonary nodules.

Keywords: Pulmonary nodules, precise early screening, malignant nodules, risk factors

Introduction

Lung cancer is a significant public health issue in China, with incidence and mortality rates among the highest globally. According to the National Cancer Center of China, lung cancer is the most common cancer in the country, accounting for about 25% of all cases [1]. The incidence has steadily risen over recent decades, largely due to the high prevalence of smoking among Chinese men, with approximately 80% of lung cancer cases attributed to tobacco use [2]. Other risk factors in China include exposure to environmental pollutants, such as air pollution, and occupational hazards, including asbestos [3]. Rapid industrialization and urbanization have worsened pollution levels, likely contributing to the high lung cancer rates [4]. Unfortunately, the prognosis for lung cancer patients in China remains poor, with a five-year survival rate of only around 15% [5], largely because the disease is often diagnosed at a late stage when treatment options are limited. Moreover, access to quality healthcare and advanced treatments can be limited in rural areas [6].

Lung cancer screening plays a critical role in the early detection and treatment of lung cancer, essential for improving patient outcomes and reducing mortality. As early-stage lung cancer often lacks noticeable symptoms, screening is crucial for early diagnosis when the disease is more treatable [7]. Detecting lung cancer at an early stage significantly increases the likelihood of curative treatment and higher survival rates [8]. Studies have demonstrated that screening can substantially lower mortality by identifying lung cancer in its early, more manageable stages [9-11]. Regular screening is particularly valu-

https://doi.org/10.62347/DTPQ4790

able for high-risk individuals, such as current or former smokers, enabling timely follow-up care and risk-reduction interventions. Early detection and treatment not only improve survival rates but also enhance patients' quality of life by reducing the disease's overall impact on their well-being [12]. While screening programs involve costs, they are often cost-effective long-term, decreasing the financial burden associated with treating advanced-stage lung cancer and contributing to improved healthcare outcomes. Additionally, lung cancer screening has broader public health benefits, alleviating the burden on healthcare systems, families, and society as a whole.

Dual-source CT is a non-invasive, relatively fast imaging modality that enables early detection of potentially malignant nodules, facilitating timely intervention and treatment decisions [13]. It also provides valuable information for follow-up and management by monitoring nodule progression or regression over time and plays a key role in lung cancer staging [14, 15]. When a malignant nodule is suspected or diagnosed, dual-source CT accurately assesses tumor extent, including spread to nearby structures and lymph nodes, which is essential for determining appropriate treatment and prognosis.

The relationship between dual-source CT parameters and clinical characteristics can be examined through quantitative analysis [16]. Previous studies suggest that biomarkers based on radiomic features correlate with clinical outcomes [17, 18]. Radiomic features are used to build diagnostic and prognostic models as clinical tools for personalized diagnosis and decision support [19]. Applying radiomics in the early screening of lung cancer may improve diagnostic accuracy and decision-making effectiveness.

This study emphasizes the importance of early and precise screening methods for pulmonary nodules, including advanced imaging techniques and novel biomarkers to improve early detection and accuracy. We also conducted an in-depth analysis of risk factors for malignant nodules, considering both traditional and potential new factors or combinations that could enhance predictive models. Additionally, innovative strategies or algorithms for distinguishing between benign and malignant nodules may be proposed based on a comprehensive factor analysis, aiming to boost diagnostic efficiency and reduce unnecessary invasive procedures. This research may further explore interdisciplinary or technological integration for more accurate assessment and management of pulmonary nodules, offering new perspectives in this field.

The current study aims to use dual-source CT parameters and clinical features to differentiate benign from malignant pulmonary nodules in the early screening of lung cancer.

Materials and methods

Clinical data

A retrospective study was conducted on 200 individuals who underwent dual-source CT lung cancer screening at the First Affiliated Hospital of Air Force Military Medical University from January to December 2023. All disease was verified through surgical specimens, with some confirmed by preoperative biopsy, including percutaneous puncture or bronchoscopic biopsy. Based on pathological reports, participants were categorized into a benign group (102 cases) and a malignant group (98 cases). Patient selection details are shown in **Figure 1**. This study received approval from the Ethics Committee of the First Affiliated Hospital of Air Force Military Medical University.

Inclusion and exclusion criteria

Inclusion criteria: (1) Age ≥ 18 years; (2) Pulmonary lesions with a maximum diameter ≤ 3 cm; (3) No prior chemotherapy, radiotherapy, or other treatments for pulmonary nodules; (4) Clear pathological diagnosis via percutaneous puncture or bronchoscopic biopsy.

Exclusion criteria: (1) Pulmonary lesions with a maximum diameter > 3 cm; (2) Presence of metastatic tumors; (3) Patients with atelectasis, pleural effusion, or mediastinal lymph node enlargement; (4) History of oral anticoagulant use.

Dual-source CT quantitative examination

Scans were performed using the Somatom Definition Flash dual-source CT scanner (Sie-

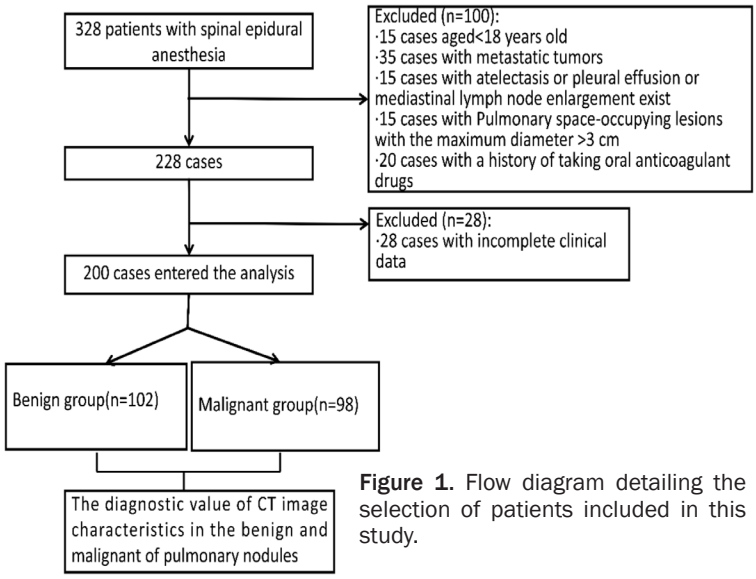

Figure 1. Flow diagram detailing the selection of patients included in this study.

mens, Germany), covering from the thoracic inlet to the mid-pole of both kidneys. Intravenous iodine hexanol (350 mgI/mL) was administered through the elbow vein at 1 mL/kg with a rate of 3.0 mL/s, followed by 30 mL of normal saline at the same rate. Scanning parameters included: Lung Nodules sequence, arterial phase (25 s), venous phase (60 s), tube voltages of 100 kV (tube A) and Sn 140 kV (tube B), with tube current-time products of 300 mAs and 232 mAs. Real-time dose adjustment (CAREDose4D) was enabled, with a rotation time of 0.5 s, collimation of 0.6 mm × 32 mm, pitch factor of 1.0, reconstructed slice thickness of 1 mm, and spacing of 1 mm. Dual-energy CT scans produced 100 kV, Sn 140 kV, and linearly fused images (M = 0.5, fusion factor). Enhanced scans in the arterial and venous phases were processed with Siemens Syngo MMWP VE40A software to generate virtual non-contrast and iodine images. Morphological lesion data were obtained after workstation processing.

Two deputy chief radiologists, working double-blinded, identified regions of interest (ROIs), avoiding calcified areas, cystic regions, hemorrhages, and obstructive lung tissue around the lesions, and measured relevant parameters. Standardized iodine concentration in the venous phase (NICvp) was calculated as the percentage ratio of iodine concentration in the lesion's venous phase (ICvp) to the concurrent iodine concentration in the internal jugular vein. Similarly, standardized iodine concentration in the arterial phase (NICAp) was the ratio of iodine concentration in the lesion's arterial phase (ICAp) to the aortic iodine concentration at the same level. Additional parameters included iodine coverage values of the lesion in the arterial phase (CTAp) and venous phase (CTvp).

Observed indicators

Dual-source CT parameters: Standardized iodine concentration in the venous phase (NICvp): calculated as the percentage ratio of iodine concentration in the lesion during the venous phase (ICvp) to that in the internal jugular vein at the same time. Standardized iodine concentration in the arterial phase (NICAp): calculated as the percentage ratio of iodine concentration in the lesion during the arterial phase (ICAp) to that in the aorta at the same level. Iodine coverage value of the lesion in the arterial phase (CTAp) and venous phase (CTvp).

Clinical data included age, gender, education level, BMI, physical activity, passive smoking exposure, family history of lung cancer, history of chronic respiratory disease, emphysema, nodule shape, longest nodule diameter, shortest nodule diameter, nodule position, density, calcification, pleural involvement, margin characteristics, and CT imaging features.

Statistical analysis

Statistical analysis was conducted using SPSS 25.0 software. The sample size was determined by power analysis and adjusted as: corrected sample size = sample size/(1-[% attrition/100]) [20], resulting in a final sample size of approximately 200. Measurement data were expressed as mean ± standard deviation, with comparisons between groups performed using the independent t-test. Count data were represented by case number and constituent ratio, with group comparisons made using the chi-square test. Ordinal data were compared using the rank-sum test. Statistical significance of differences between dual-source CT and clini-

cal characteristics in the two groups was assessed, along with accuracy, sensitivity, and specificity calculations. Using pathological diagnosis as the "gold standard", the receiver operating characteristic (ROC) curve was applied to determine the area under the curve (AUC) and evaluate the diagnostic efficacy of different examinations for pulmonary nodule characterization. Statistical significance was set at $P < 0.05$.

Results

Comparison of baseline characteristics

In the benign group, there were 59 males and 43 females, aged 19-73 years, with an average disease duration of 59.21±7.65 years. In the malignant group, there were 55 males and 43 females, aged 19-78 years, with an average disease duration of 58.23±7.69 years. No significant differences were observed in age, gender, education level, BMI, physical activity, passive smoking, family history of lung cancer, chronic respiratory disease history, emphysema, or nodule shape (all $P > 0.05$). Significant differences, however, were found in longest and shortest nodule diameters, position, density, calcification, pleural involvement, and margin characteristics (all $P < 0.05$) (**Table 1**).

CT imaging features

In the CT lung window images of benign pulmonary nodules, a mixed ground-glass nodule with a centrally located, regular solid component that is not connected to blood vessels is observed (**Figure 2A**, **2B**). In contrast, the lung window image of a malignant nodule shows a mixed ground-glass nodule with an eccentrically located, regular solid component that is connected to blood vessels (**Figure 2C**, **2D**).

Comparison of CT imaging features

In terms of CT imaging features, the lobulation rate was 21.57% in the benign group and 78.57% in the malignant group, showing a significant difference ($P < 0.001$). The burr sign was present in 14.71% of the benign group and 61.22% of the malignant group ($P < 0.001$). Pleural indentation was observed in 4.90% of the benign group and 37.76% of the malignant group ($P = 0.002$). Calcification was present in 39.22% of the benign group but absent in the malignant group ($P = 0.001$). The vascular cluster sign was seen in 4.90% of benign cases and 48% of malignant cases, also indicating a significant difference ($P < 0.001$) (**Table 2**).

Comparison of quantitative parameters

The NICvp in the malignant group was 30.25± 46.7, while in the benign group, it was 31.24± 4.45, with no significant difference ($P = 0.147$). The CTvp was 30.27±53.4 in the malignant group and 31.87±5.78 in the benign group, again showing no significant difference ($P = 0.224$). However, the NICAp was significantly higher in the malignant group (13.54±4.12) compared to the benign group (6.67±1.75) ($P = 0.002$). Similarly, the CTAp was higher in the malignant group (24.57±6.67) versus the benign group (15.57±3.67) ($P = 0.001$) (**Table 3**).

Comparison of CT examinations

The diagnostic accuracy of chest CT for distinguishing benign and malignant nodules was 88.78% (87/98), with a sensitivity of 44.90% (44/98) and a specificity of 57.84% (59/102). The positive detection rate of CT was 42.16% (43/102) in the benign group and 44.90% (44/98) in the malignant group. Chi-square testing indicated a significant difference in positive detection rates between the groups ($P = 0.033$), suggesting a higher positive detection rate in the malignant group (**Table 4**).

Univariate and multivariate logistic regression analysis

Univariate analysis included factors were those such as pleural involvement, nodule margin, burr sign, pleural indentation, lobulation, hemoglobin, antiphospholipid antibody, calcification, nodule density, solid nodule, NICAp, CTAp, longest and shortest nodule diameters, and nodule position. The results showed that solid nodule (95% CI 1.341-3.014; $P = 0.015$), NICAp (95% CI 1.354-3.137; $P = 0.001$), CTAp (95% CI 1.321-8.247; $P = 0.004$), longest nodule diameter (95% CI 1.119-9.398; $P = 0.017$), and shortest nodule diameter (95% CI 1.011-3.209; $P = 0.007$) were significantly different (**Table 5**). These factors were then included in a multivariate analysis, which identified NICAp (95% CI

Table 1. Comparison of baseline characteristics between the two groups

Risk factor	Benign group (n = 102)	Malignant group (n = 98)	χ^2/t	P
Age	59.21±7.65	58.23±7.69	0.187	0.122
Sex			0.060	0.806
Male	59 (57.84%)	55 (56.12%)		
Female	43 (42.16%)	43 (43.88%)		
Educational level			0.105	0.949
Low	24 (23.53%)	23 (23.47%)		
Medium	64 (62.75%)	60 (61.22%)		
High	14 (13.72%)	15 (15.31%)		
BMI			1.705	0.636
< 18.5	3 (2.94%)	6 (6.12%)		
18.5-24	52 (50.98%)	50 (51.02%)		
24-28	39 (38.24%)	37 (37.76%)		
≥ 28	8 (7.84%)	5 (5.10%)		
Frequent movement	28 (27.45%)	22 (22.45%)	0.667	0.414
Years of passive smoking			0.091	0.993
No	19 (18.63%)	18 (18.37%)		
0-19	12 (11.76%)	11 (11.22%)		
20-39	50 (49.02%)	50 (51.02%)		
≥ 40	21 (20.59%)	19 (19.39%)		
Smoking	66 (64.71%)	64 (65.31%)	0.008	0.929
Family history of lung cancer	52 (50.98%)	56 (66.33%)	0.764	0.382
History of chronic respiratory disease	72 (70.59%)	68 (69.39%)	0.034	0.853
Emphysema	11 (10.78%)	11 (11.22%)	0.010	0.921
Tubercle length	9.36±7.04	20.65±14.26	10.221	< 0.001
Tuberous minor diameter	6.97±4.82	15.87±10.28	9.891	< 0.001
Nodule position			23.884	0.000
Not the superior lobe of the lung	64 (62.75%)	90 (91.84%)		
Superior lobe of the lung	38 (37.25%)	8 (8.16%)		
Nodule density			15.701	0.000
Substantiality	77 (75.49%)	53 (54.08%)		
Partial reality	15 (14.71%)	30 (30.61%)		
Imreality	10 (9.80%)	25 (25.51%)		
Nodular calcification	14 (13.73%)	3 (3.06%)	6.172	0.013
Whether the nodules are pleural involved	19 (18.63%)	48 (48.98%)	20.668	0.000
Nodular margin			6.418	0.011
Smooth	68 (66.67%)	48 (48.98%)		
Burr	34 (33.33%)	50 (51.02%)		
Nodule shape			0.007	0.934
Roundness	94 (92.16%)	90 (91.84%)		
Ellipse	8 (7.84%)	8 (8.16%)		

1.045-1.367; P = 0.007), CTAp (95% CI 1.341-4.123; P = 0.005), solid nodule (95% CI 1.198-2.978; P = 0.008), and nodule density (95% CI 1.128-2.987; P = 0.007) as independent diagnostic factors for malignant nodules (**Table 6**).

ROC analysis

The ROC analysis revealed that NICAp had a sensitivity of 92.4% and specificity of 84.9% for predicting malignant nodules. CTAp demon-

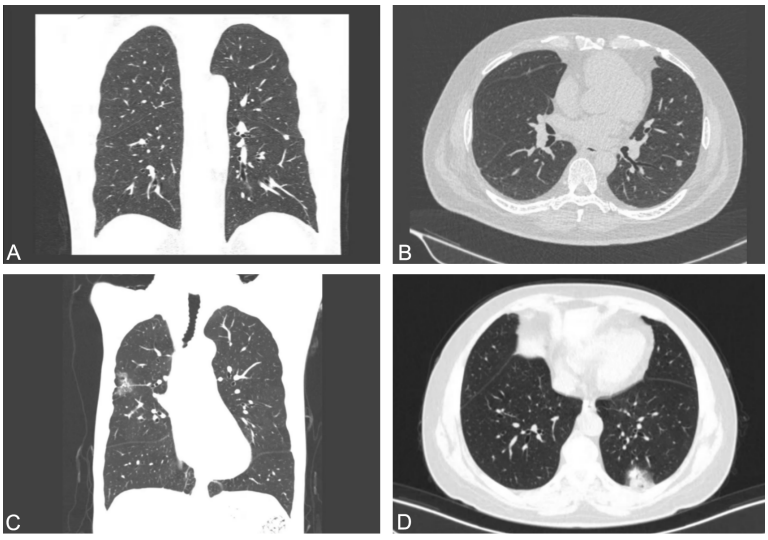

Figure 2. CT imaging features of the two groups. A, B. In the CT lung window images of a benign pulmonary nodule reveal a mixed ground-glass nodule. The solid component has a regular shape, centrally distributed, and is not connected to the blood vessels. C, D. CT lung window images of a malignant pulmonary nodule show a mixed ground-glass nodule with a solid component that has a regular shape but is eccentrically distributed and connected to blood vessels.

strated a sensitivity of 93.4% and specificity of 80.1%. The sensitivity and specificity for predicting malignant nodules based on solid nodule presence were 78.8% and 81.8%, respectively. For nodule density, the sensitivity was 79.9% and specificity was 80.3% (**Table 7** and **Figure 3**).

Discussion

This study found that NICAP and CTAP values were significantly higher in patients with malignant pulmonary nodules compared to those with benign nodules. Univariate and multivariate analyses identified NICAp, CTAp, solid nodule, and nodule density as independent diagnostic factors for malignancy.

NICAp was shown to be an independent diagnostic factor for malignant nodules. During the development of lung cancer, abnormal angiogenesis leads to the formation of new blood vessels that differ significantly from normal vasculature. NICAp reflects the iodine uptake and distribution within the lesion during the venous phase, correlating closely with the tumor's blood supply characteristics [21]. Malignant nodules often exhibit enhanced angiogenesis, increasing vessel density and vascular permeability. This results in a higher iodine concentration in malignant nodules than in benign ones [22, 23]. NICAp measurement thus provides valuable diagnostic information, with this study confirming NICAp (95% CI 1.045-1.367; P = 0.007) as a significant diagnostic factor for malignancy.

CTAp was also identified as an independent diagnostic factor for malignant nodules. In these nodules, abnormal angiogenesis occurs, driven by various tumor-secreted factors that promote new blood vessel formation [24]. During the arterial phase of contrast-enhanced CT, malignant nodules receive a more substantial blood supply, leading to increased iodine uptake and higher coverage values [25]. Additionally, malignant nodules often display altered microvascular architecture, including more tortuous, dilated vessels with increased permeability [26]. These vascular changes permit more contrast agent to enter the lesion during the arterial phase, further elevating the iodine coverage value [27]. Malignant nodules' increased metabolic activity and demand for nutrients and oxygen are also reflected in the enhanced arterial-phase iodine uptake [28].

We also demonstrated that solid nodules can assist in diagnosing malignant nodules. Malignant cells actively proliferate, forming dense masses that appear as solid nodules, thereby increasing the suspicion of malignancy [29]. The unregulated growth and biological behavior of malignant cells contribute to the formation of these solid structures, which may also exhibit angiogenesis to support their nutrient and oxygen requirements [30]. Additionally, molecular changes and microenvironmental alterations within the nodules influence the development of solid nodules, further indicating malignancy [31, 32]. Unlike benign nodules, solid nodules often display more complex and irregular internal structures and distinct cellular composition, both associated with malignant transformation [33].

Table 2. Comparison of CT imaging features between the two groups

Image feature	Benign group (n = 102)	Malignant group (n = 98)	χ^2/Z	p
Diameter			0.869	0.648
0-10 mm	21 (20.59%)	20 (20.14%)		
11-20 mm	45 (44.12%)	49 (50.00%)		
21-30 mm	36 (35.29%)	29 (29.86%)		
Shape			0.905	0.341
Circle/quasi-circle	72 (70.59%)	63 (64.29%)		
Irregularity	30 (29.41%)	35 (35.71%)		
Position			3.504	0.061
Superior lobe	49 (48.04%)	60 (61.22%)		
Other leaf	53 (51.96%)	38 (38.78%)		
Lobulation	22 (21.57%)	77 (78.57%)	64.967	0.000
Burr sign	15 (14.71%)	60 (61.22%)	46.146	0.000
Pleural indentation	5 (4.90%)	37 (37.76%)	32.516	0.000
Calcification	40 (39.22%)	8 (8.16%)	26.422	0.000
Bronchial amputation sign	15 (14.71%)	14 (14.29%)	0.007	0.933
Boundary			0.028	0.867
Clear	93 (91.18%)	90 (91.84%)		
Blur	9 (8.82%)	8 (8.16%)		
Cavity sign	15 (14.71%)	17 (17.35%)	0.259	0.611
Vascular cluster sign	5 (4.90%)	47 (48.00%)	48.160	0.000
Nodule density			46.162	0.000
Solid nodule	93 (91.18%)	46 (46.94%)		
Mix ground glass nodules	5 (4.90%)	27 (27.55%)		
Pure ground glass nodules	4 (3.92%)	25 (25.51%)		

Table 3. Comparison of quantitative parameters of between the two groups

	Malignant group (n = 98)	Benign group (n = 102)	F	P
NICvp	30.25±46.7	31.24±4.45	1.397	0.147
CTvp	30.27±53.4	31.87±5.78	1.234	0.224
NICAp	13.54±4.12	6.67±1.75	12.874	0.002
CTAp	24.57±6.67	15.57±3.67	9.987	0.001

Note: NICvp: Dual-source CT parameters included Standardized iodine concentration in the venous phase; CTvp: iodine coverage value of the lesion in the venous phase; NICAp: standardized iodine concentration in the arterial phase; CTAp: iodine coverage value of the lesion in the arterial phase.

Table 4. Comparison of CT examinations between two the groups

CT diagnosis	Benign group (n = 102)	Malignant group (n = 98)	Total
Positive	43	44	87
Negative	59	54	113
Total	102	98	200

Nodule density is also an independent diagnostic factor for malignant nodules. Solid nodules often have relatively high density, with some malignant nodules showing densities that differ from benign ones [34]. The irregular, aggressive growth pattern of malignant cells typically results in a more compact and dense structure [35]. Certain malignant nodules may exhibit areas of necrosis or calcification, providing additional diagnostic clues [36]. Interactions

Table 5. Univariate logistic regression analysis

Index	β	SE	Wald	P	OR (95% CI)
Whether the nodules are pleural involved	-0.048	0.145	0.117	0.741	0.987 (0.718-0.129)
Nodular margin	-0.074	0.078	0.365	0.423	0.954 (0.748-1.127)
Burr sign	-1.068	0.746	2.074	0.152	0.348 (0.087-1.424)
Pleural indentation	-1.068	0.743	2.074	0.152	0.348 (0.087-1.424)
Lobulation	0.041	0.003	2.536	0.123	1.008 (0.987-1.007)
calcification	0.007	0.008	0.654	0.113	1.007 (0.997-1.526)
Nodule density	0.224	0.097	5.587	0.428	1.247 (1.038-1.547)
Solid nodule	0.714	0.225	10.254	0.015	2.047(1.341-3.014)
NICAp	0.701	0.223	9.987	0.001	2.047 (1.354-3.137)
CTAp	1.287	0.268	9.912	0.004	3.569 (1.321-8.247)
Tubercle length	1.578	0.247	15.874	0.017	2.123 (1.119-9.398)
Nodule density	0.107	0.278	0.669	0.827	1.169 (0.587-1.698)
Tuberous minor diameter	-0.854	0.187	10.267	0.007	1.365 (1.011-3.209)
Nodule position	0.224	0.357	0.749	0.477	1.287 (0.624-2.004)

Note: NICAp: standardized iodine concentration in the arterial phase; CTAp: iodine coverage value of the lesion in the arterial phase.

Table 6. Multivariate logistic regression analysis

Index	β	SE	Wald	P	OR (95% CI)
NICAp	0.179	0.056	7.259	0.007	1.178 (1.045-1.367)
CTAp	0.854	0.287	8.547	0.005	2.354 (1.341-4.123)
Solid nodule	0.598	0.247	7.852	0.008	1.874 (1.198-2.978)
Nodule density	0.657	0.228	8.559	0.007	1.987 (1.128-2.987)

Note: NICAp: standardized iodine concentration in the arterial phase; CTAp: iodine coverage value of the lesion in the arterial phase.

Table 7. ROC curve analysis for early diagnosis of malignant nodules by CT examinations

Factor	AUC	Sensitivity	Specificity	P
NICAp	0.875	92.4	84.9	0.002
CTAp	0.878	93.4	80.1	0.001
Solid nodule	0.786	78.8	81.8	0.004
Nodule density	0.788	79.9	80.3	0.003

Note: NICAp: standardized iodine concentration in the arterial phase; CTAp: iodine coverage value of the lesion in the arterial phase.

between tumor cells and the surrounding stroma can also influence density characteristics, adding to the distinct presentation of malignant nodules [37].

This study does have a few limitations. First, the sample size was relatively small, which could affect the generalizability of the findings. Second, the criteria for early screening and identification of pulmonary nodules may not be comprehensive, potentially missing subtle or specific cases. Additionally, some potential risk factors for malignant nodules were not fully explored, leading to an incomplete understanding. The study's setting and population might introduce bias, which should be considered when interpreting the results. Future research should include a larger sample size to gather more comprehensive and accurate data, enhancing the reliability and applicability of the findings.

In conclusion, our findings indicate that NICAp, CTAp, solid nodule, and nodule density are

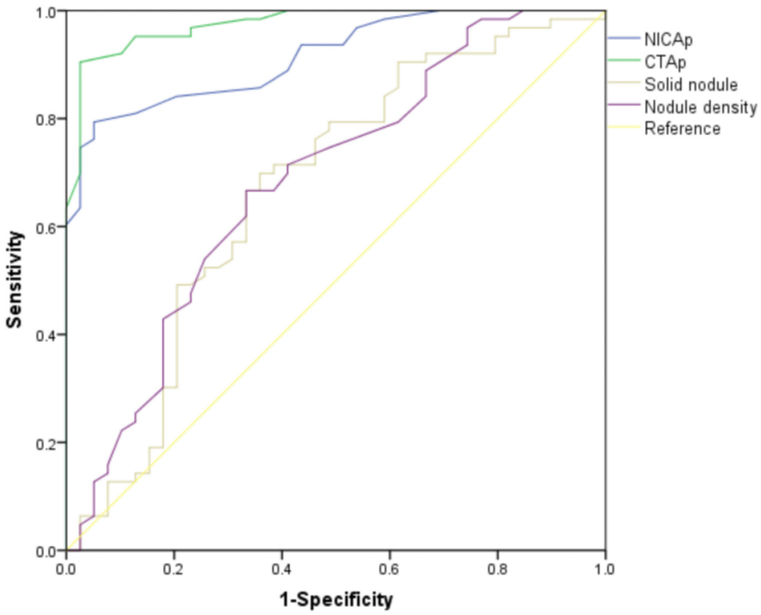

Figure 3. ROC curve analysis for early diagnosis of malignant nodules by CT examinations. NICAp: standardized iodine concentration in the arterial phase; CTAp: iodine coverage value of the lesion in the arterial phase.

independent diagnostic factors for malignant nodules and serve as predictors in distinguishing benign from malignant lung nodules.

Disclosure of conflict of interest

None.

Address correspondence to: Teng Wang, Health Management Center, Weinan Central Hospital, Middle Section of Shengli Street, Linwei District, Weinan 714000, Shaanxi, China. Tel: +86-1509-1131621; E-mail: 15929337600@163.com

References

[1] Bray F, Laversanne M, Sung H, Ferlay J, Siegel RL, Soerjomataram I and Jemal A. Global cancer statistics 2022: GLOBOCAN estimates of incidence and mortality worldwide for 36 cancers in 185 countries. CA Cancer J Clin 2024; 74: 229-263.

[2] Zhao J, Shi YL, Wang YT, Ai FL, Wang XW, Yang WY, Wang JX, Ai LM, Hu KR and Wan X. Lung cancer risk attributable to active smoking in China: a systematic review and meta-analysis. Biomed Environ Sci 2023; 36: 850-861.

[3] He S, Li H, Cao M, Sun D, Lei L, Li N, Peng J and Chen W. Trends and risk factors of lung cancer in China. Chin J Cancer Res 2020; 32: 683-694.

[4] Li J, Lu X, Liu F, Liang F, Huang K, Yang X, Xiao Q, Chen J, Liu X, Cao J, Chen S, Shen C, Yu L, Lu F, Wu X, Zhao L, Wu X, Li Y, Hu D, Huang J, Zhu M, Liu Y, Shen H and Gu D. Chronic effects of high fine particulate matter exposure on lung cancer in China. Am J Respir Crit Care Med 2020; 202: 1551-1559.

[5] Ma W, Zeng J, Montoya DJ, Toomey K, Zhou C, Chen S, Liu D, Babich M, Radosevich JA and Li T. Labyrinthin expression is associated with poor prognosis in patients with non-small-cell lung cancer. Cancers (Basel) 2023; 15: 924.

[6] Li K, Li L, Wu X, Yu J, Ma H, Zhang R, Li Y and Wang W. Loss of SDC1 expression is associated with poor prognosis of colorectal cancer patients in northern China. Dis Markers 2019; 2019: 3768708.

[7] Tammemägi MC, Darling GE, Schmidt H, Walker MJ, Langer D, Leung YW, Nguyen K, Miller B, Llovet D, Evans WK, Buchanan DN, Espino-Hernandez G, Aslam U, Sheppard A, Lofters A, McInnis M, Dobranowski J, Habbous S, Finley C, Luettschwager M, Cameron E, Bravo C, Banaszewska A, Creighton-Taylor K, Fernandes B, Gao J, Lee A, Lee V, Pylypenko B, Yu M, Svara E, Kaushal S, MacNiven L, McGarry C, Della Mora L, Koen L, Moffatt J, Rey M, Yurcan M, Bourne L, Bromfield G, Coulson M, Truscott R and Rabeneck L. Risk-based lung cancer screening performance in a universal healthcare setting. Nat Med 2024; 30: 1054-1064.

[8] Fitzgerald RC, Antoniou AC, Fruk L and Rosenfeld N. The future of early cancer detection. Nat Med 2022; 28: 666-677.

[9] Leiter A, Veluswamy RR and Wisnivesky JP. The global burden of lung cancer: current status and future trends. Nat Rev Clin Oncol 2023; 20: 624-639.

[10] Wu JT, Wakelee HA and Han SS. Optimizing lung cancer screening with risk prediction: current challenges and the emerging role of biomarkers. J Clin Oncol 2023; 41: 4341-4347.

[11] Bernstein E, Lev-Ari S, Shapira S, Leshno A, Sommer U, Al-Shamsi H, Shaked M, Segal O, Galazan L, Hay-Levy M, Sror M, Harlap-Gat A, Peer M, Moshkowitz M, Wolf I, Liberman E, Shenberg G, Gur E, Elran H, Melinger G, Mashiah J, Isakov O, Zrifin E, Gluck N, Dekel R, Kleinman S, Aviram G, Blachar A, Kessler A, Golan O, Geva R, Yossepowitch O, Neugut AI and Ar-

ber N. Data from a one-stop-shop comprehensive cancer screening center. J Clin Oncol 2023; 41: 2503-2510.
[12] Tammemägi MC, Ruparel M, Tremblay A, Myers R, Mayo J, Yee J, Atkar-Khattra S, Yuan R, Cressman S, English J, Bedard E, MacEachern P, Burrowes P, Quaife SL, Marshall H, Yang I, Bowman R, Passmore L, McWilliams A, Brims F, Lim KP, Mo L, Melsom S, Saffar B, Teh M, Sheehan R, Kuok Y, Manser R, Irving L, Steinfort D, McCusker M, Pascoe D, Fogarty P, Stone E, Lam DCL, Ng MY, Vardhanabhuti V, Berg CD, Hung RJ, Janes SM, Fong K and Lam S. USPSTF2013 versus PLCOm2012 lung cancer screening eligibility criteria (international lung screening trial): interim analysis of a prospective cohort study. Lancet Oncol 2022; 23: 138-148.
[13] Almeida IP, Schyns LE, Öllers MC, van Elmpt W, Parodi K, Landry G and Verhaegen F. Dual-energy CT quantitative imaging: a comparison study between twin-beam and dual-source CT scanners. Med Phys 2017; 44: 171-179.
[14] Sauranen S, Mäkelä T, Kaasalainen T and Kortesniemi M. Dual-energy computed tomography quality control: initial experiences with a semi-automatic analysis tool. Phys Med 2024; 118: 103211.
[15] Zhang YP, Heuvelmans MA, Zhang H, Oudkerk M, Zhang GX and Xie XQ. Changes in quantitative CT image features of ground-glass nodules in differentiating invasive pulmonary adenocarcinoma from benign and in situ lesions: histopathological comparisons. Clin Radiol 2018; 73: 504.e9-504.e16.
[16] Patel J, Klopper J and Cottrill EE. Molecular diagnostics in the evaluation of thyroid nodules: current use and prospective opportunities. Front Endocrinol (Lausanne) 2023; 14: 110-1410.
[17] Xu M, Zeng S, Li F and Liu G. Utilizing grayscale ultrasound-based radiomics nomogram for preoperative identification of triple negative breast cancer. Radiol Med 2024; 129: 29-37.
[18] Jiang M, Yang P, Li J, Peng W, Pu X, Chen B, Li J, Wang J and Wu L. Computed tomography-based radiomics quantification predicts epidermal growth factor receptor mutation status and efficacy of first-line targeted therapy in lung adenocarcinoma. Front Oncol 2022; 12: 985284.
[19] Guiot J, Vaidyanathan A, Deprez L, Zerka F, Danthine D, Frix AN, Lambin P, Bottari F, Tsoutzidis N, Miraglio B, Walsh S, Vos W, Hustinx R, Ferreira M, Lovinfosse P and Leijenaar RTH. A review in radiomics: making personalized medicine a reality via routine imaging. Med Res Rev 2022; 42: 426-440.
[20] Mazzone PJ and Lam L. Evaluating the patient with a pulmonary nodule: a review. JAMA 2022; 327: 264-273.
[21] Khodayari Moez E, Warkentin MT, Brhane Y, Lam S, Field JK, Liu G, Zulueta JJ, Valencia K, Mesa-Guzman M, Nialet AP, Atkar-Khattra S, Davies MPA, Grant B, Murison K, Montuenga LM, Amos CI, Robbins HA, Johansson M and Hung RJ. Circulating proteome for pulmonary nodule malignancy. J Natl Cancer Inst 2023; 115: 1060-1070.
[22] Hammer MM. Risk and time to diagnosis of lung cancer in incidental pulmonary nodules. J Thorac Imaging 2024; 39: 275-280.
[23] Bai GY, Qiu B, Ji Y, Song P, Zhang F, Xue Q and Gao SG. Progress in diagnosis and treatment of lung adenocarcinomas imaging manifesting as radiological part-solid nodule. Zhonghua Zhong Liu Za Zhi 2021; 43: 743-750.
[24] Zhu T, Xie K, Wang C, Wang L, Liu W and Zhang F. Diagnostic effectiveness of dual source dual energy computed tomography for benign and malignant thyroid nodules. Evid Based Complement Alternat Med 2022; 2022: 2257304.
[25] Iacobellis F, Scaglione M, Brillantino A, Scuderi MG, Giurazza F, Grassi R, Noschese G, Niola R, Al Zuhir NYS and Romano L. The additional value of the arterial phase in the CT assessment of liver vascular injuries after high-energy blunt trauma. Emerg Radiol 2019; 26: 647-654.
[26] Ma H, Guo H, Zhao M, Qi S, Li H, Tian Y, Li Z, Zhang G, Yao Y and Qian W. Automatic pulmonary ground-glass opacity nodules detection and classification based on 3D neural network. Med Phys 2022; 49: 2555-2569.
[27] Westöö C, Norvik C, Peruzzi N, van der Have O, Lovric G, Jeremiasen I, Tran PK, Mokso R, de Jesus Perez V, Brunnström H, Bech M, Galambos C and Tran-Lundmark K. Distinct types of plexiform lesions identified by synchrotron-based phase-contrast micro-CT. Am J Physiol Lung Cell Mol Physiol 2021; 321: L17-L28.
[28] Wang Z, Yang L, Wang W, Zhou H, Chen J, Ma Z, Wang X, Zhang Q, Liu H, Zhou C, Guo Z and Zhang X. Comparative immunological landscape between pre- and early-stage LUAD manifested as ground-glass nodules revealed by scRNA and scTCR integrated analysis. Cell Commun Signal 2023; 21: 325.
[29] Paulinelli RR, Oliveira LF, Freitas-Junior R and Soares LR. The accuracy of the SONOBREAST statistical model in comparison to BI-RADS for the prediction of malignancy in solid breast nodules detected at ultrasonography. Eur J Obstet Gynecol Reprod Biol 2016; 196: 1-5.
[30] Xiang P, Ahmadi S, Coleman A, West W, Lobon I, Bikas A, Landa I, Marqusee E, Kim M, Alexander EK and Pappa T. Identifying and predicting

diverse patterns of benign nodule growth. J Clin Endocrinol Metab 2023; 108: e458-e463.
[31] Hammer MM, Palazzo LL, Kong CY and Hunsaker AR. Cancer risk in subsolid nodules in the national lung screening trial. Radiology 2019; 293: 441-448.
[32] Remsik J and Boire A. The path to leptomeningeal metastasis. Nat Rev Cancer 2024; 24: 448-460.
[33] Wu S, Fan X, Li X, Luo TY, Li XH and Li Q. Clinical and non-contrast computed tomography characteristics and disease development in patients with benign pulmonary subsolid nodules with a solid component ≤5 mm. Insights Imaging 2024; 15: 6.
[34] Kobayashi H, Ohkubo M, Narita A, Marasinghe JC, Murao K, Matsumoto T, Sone S and Wada S. A method for evaluating the performance of computer-aided detection of pulmonary nodules in lung cancer CT screening: detection limit for nodule size and density. Br J Radiol 2017; 90: 20160313.
[35] Orzan OA, Dorobanțu AM, Gurău CD, Ali S, Mihai MM, Popa LG, Giurcăneanu C, Tudose I and Bălăceanu B. Challenging patterns of atypical dermatofibromas and promising diagnostic tools for differential diagnosis of malignant lesions. Diagnostics (Basel) 2023; 13: 671.
[36] Petković M and Jurakić Tončić R. Nested melanoma, a new morphological variant of superficial spreading melanoma with characteristic dermoscopic features. Acta Dermatovenerol Croat 2017; 25: 80-81.
[37] Xu M, Zhang T, Xia R, Wei Y and Wei X. Targeting the tumor stroma for cancer therapy. Mol Cancer 2022; 21: 208.